Available online at www.sciencedirect.com

SciVerse ScienceDirect

Ceramics International 39 (2013) 5741–5750

CERAMICS INTERNATIONAL

www.elsevier.com/locate/ceramint

Removal of iron from $BaTa_2O_6$ ceramic powder produced by high energy milling

Mustafa İlhan[a], Ayhan Mergen[a,*], Cemalettin Yaman[b]

[a]Department of Metallurgical and Materials Engineering, Marmara University, Göztepe Campus, 34722 Kadiköy, İstanbul, Turkey
[b]Department of Metallurgical and Materials Engineering, Yildiz Technical University, 34220 Davutpaşa-İstanbul, Turkey

Received 6 November 2012; received in revised form 22 December 2012; accepted 31 December 2012
Available online 23 January 2013

Abstract

In order to remove Fe coming from the milling environment, mechanochemically produced $BaTa_2O_6$ ceramic powder was leached with 6 and 12 M HCl at 95 °C and 105 °C for time periods varying between 1 and 15 h. Amount of Fe in leached samples was determined by EDS and XRF. Fe concentration decreased from 10.36% to 1.97–3.16% after leaching indicating a 70–81% decrease in iron. Leaching temperature had a more pronounced effect on iron removal than concentration. Leaching caused the formation of porosities and disintegration of powder which accelerated the iron removal. X-ray diffraction analysis of leached milled powders heat treated between 1000 and 1450 °C for 5 h indicated that although iron related phases were formed above 1000 °C, single $BaTa_2O_6$ phase was obtained at 1425 °C having tetragonal tungsten bronze type structure. A possible liquid phase formation above 1300 °C led to an increase in grain size and density.

Keywords: A.Sintering; Mechanochemical synthesis; Leaching; SEM

1. Introduction

$BaO–Ta_2O_5$ system has interesting properties due to its dielectric and especially photocatalytic properties [1–4]. To solve the energy problems and to meet the demand of environmental clean-up, photocatalysis is currently applied [5,6]. For this purpose, design and preparation of efficient photocatalytic materials are substantial [7]. Heterogeneous photocatalysis has a great potential for converting photon energy into chemical energy and for decomposing pollutants in air or solution [8,9]. $BaTa_2O_6$ is used in electro-optics and it is one of the alkaline and alkaline earth tantalates exhibiting high photocatalytic properties [3,10,11]. $BaTa_2O_6$ have three polymorphs; a low-temperature orthorhombic form under 1150 °C transforms to tetragonal form between 1150 and 1300 °C and the hexagonal form above 1300 °C [1,2,4]. Photocatalytic properties of $BaTa_2O_6$ having orthorhombic form are higher than the other forms of tetragonal or hexagonal [3].

Although high energy milling has advantages over conventional mixed oxide techniques like higher degree of homogeneity, lower sintering temperature without calcination step, lower particle size and improved properties, it is faced with a serious contamination problem which has impeded the progress of this method [12]. During high-energy milling the ball–powder–ball collision in a tumbling, planetary, or vibrating mill can be the main source of iron contamination [13]. The magnitude of contamination depends on the time of milling, the intensity of milling, the atmosphere in which the powder is milled, and the difference in the strength/hardness of the powder and the milling medium [14]. Contamination levels during milling of different types of powders for various mills strongly varied depending on the type of grinding medium (Table 1). Although Fe contamination was commonly between 1 and 4 wt% for steel grinding medium [14], amounts as large as 22 wt% Fe in a W–C mixture milled for 310 h [15] and 13.31 wt% Fe in pure W milled for 50 h in a SPEX mill were also reported [16]. In a previous study, mechanochemical synthesis of $BaTa_2O_6$ ceramic powder resulted in 10.36% Fe contamination as a result of 10 h of high-energy milling in a planetary mill [12].

*Corresponding author. Tel.: +90 216 348 02 92x603; Fax: +90 216 345 01 26.
E-mail address: ayhan.mergen@marmara.edu.tr (A. Mergen).

0272-8842/$ - see front matter © 2012 Elsevier Ltd and Techna Group S.r.l. All rights reserved.
http://dx.doi.org/10.1016/j.ceramint.2012.12.092

Table 1
Contamination levels of different types of powders in various mills depending on milling medium, milling time and ball/powder ratio.

Milling system	Milling type	Milling medium (Vial, Balls)	Milling time (h)	Ball/ powder Ratio	Fe contamiation wt (%)	Refs.
$BaCO_3 + Ta_2O_5$	Planetary	Stainless steel	10	40:1	10.36	[12, present work]
W	SPEX	Stainless steel	50	4:1	13.31	[15]
W+C	SPEX	Stainless steel	310	30:1	22	[16]
$TiOSO_4 \cdot xH_2O + Na_2CO_3$	Planetary	Stainless steel	1	20:1	3	[17]
$Ti + TiO_2$	Planetary	Hardened steel	2	30:1	2	[18]
$V_2O_5 + 4C + N_2$	Planetary	Steel	8	16:1	8.9	[19]
$CoCl_2 + FeCl_2 + NaOH$	Planetary	Hardened steel	62	10:1	10	[20]
Al_2O_3	SPEX	Stainless steel	32	10:1	11	[21]
Al_2O_3	SPEX	WC	32	10:1	34.7	[21]
Al_2O_3	SPEX	ZrO_2	32	10:1	1.5	[21]
Nb	Planetary	WC	40	10:1	12	[22]
Nb+92Be	SPEX	WC–Co	60	7:1	0	[23]

Chloride hydrometallurgy has been extensively applied for the removal of iron [24,25]. HCl, as a leaching agent, is preferred to other acids due to its relatively easier recovery of the useful free acid from its waste solution, its practicability at moderate temperature solubilizing all metals, easy separation of iron as precipitate and high degree of solubility of metal chlorides than the corresponding salts [26]. Furthermore, the recovery of a number of metal ions by liquid–liquid extraction from hydrochloric acid solution is considerably easier than from sulfuric acid (H_2SO_4) solutions [27,28]. In addition, chloride based system has advantages over sulfate based leaching in that elemental sulfur resulting from the oxidation potential of ferric chloride leaching system is an environmentally more acceptable product compared to the sulfur dioxide from pyrometallurgy or sulfate from H_2SO_4 leaching [26]. Various studies have been reported on the removal of iron impurity by HCl leaching. In these studies, effect of stirring speed, particle size, temperature, acid concentration, and liquid/solid ratio on the kinetics of dissolution of solid in hydrochloric acid has been studied (Table 2). In a study made by Mergen [29] the Fe content was reduced from about 18.49% Fe_2O_3 to 1.3 wt% after 6 h of leaching using 6 M HCl at 60 °C. Temuujin et al. [30] leached the vermiculite containing 8.88% Fe_2O_3 using 2 M HCl for 2 h at 80 °C and decreased the iron to 0.28%.

2. Experimental

$BaTa_2O_6$ ceramic powder was produced by mechanochemical synthesis using starting materials of $BaCO_3$ (Fluka, 98.5%) and Ta_2O_5 (Alfa Aesar, 99%). After mixing the starting materials in an agate mortar, they were high energy milled in a planetary ball mill (Fritsch Pulverisette 5) in a stainless steel vial using stainless steel balls at a speed of 280 rpm/min using ball/powder ratio of 40:1. $BaTa_2O_6$ powder was produced after 10 h of milling. The details of the synthesis method were given elsewhere [12].

The synthesized $BaTa_2O_6$ ceramic powder was leached using 6 and 12 M HCl solutions at 95 °C and 105 °C for various time periods (1 to 15 h) at a mixing speed of 300 rpm to remove iron from the powder. Although leaching was performed using 6 and 12 M HCl concentrations, it should be taken into consideration that acid concentration was not stable due to HCl evaporation at 95 °C and 105 °C during the reaction. Samples were collected at various time intervals during leaching to monitor the Fe content of the powder which was analyzed by energy dispersive spectrometer (EDS) in the SEM. In addition, iron content and weight fractions of other elements in milled and leached powder were also checked with an X-ray fluorescence spectrometer (XRF). In order to acquire accurate values, EDS analysis was carried out on 10 different points on each sample and average values were taken [34,35]. The spot size of electron beam was about 1 mm^2 and the measurement period was 120 s. The electron microscope was operated at 20 kV for EDS analysis. After determining the optimum leaching conditions in terms of time, temperature and molarities, $BaTa_2O_6$ powder was leached at these conditions and then the powder was made into a pellet at 1 MPa pressure ($\sim$102 t/m^2). Ceramic pellets were sintered between 1000 and 1450 °C for 5 h with heating and cooling rates of 250 °C/h. The density of the pellets was measured by Archimedes' method.

The morphology of the powders and fracture surfaces of the sintered ceramics were investigated by a scanning electron microscope (SEM, JEOL Ltd., JSM-5910LV) equipped with EDS (OXFORD Industries INCAx-Sight 7274; 133 eV resolution 5.9 keV) after gold coating. Elemental weight percentages of the milled and leached powder were determined by an X-ray fluorescence spectrometer (XRF, Rigaku Corp., ZSX mini-Pd Target). Phase compositions in leached and sintered samples were determined by an X-ray diffractometer (XRD, Rigaku Corp., D-MAX 2200) using Cu Kα radiation at a scan rate of 1°/min between 2θ: 20° and 60°.

3. Results and discussion

3.1. Leaching of $BaTa_2O_6$

$BaTa_2O_6$ ceramic powders were successfully produced by mechanochemical synthesis after 10 h of high energy milling. XRF analysis of this powder indicated that BaO

Table 2
Acid leaching studies for iron removal depending on acid concentration, temperature, time, stirring speed, particle size and liquid/solid ratio.

System	Acid concentration (M)	Temperature(C°)	Time (h)	Effect of stirring speed (rpm)	Particle size (μm)	Solid: liquid ratio (g/L)	Fe% before leach ing	Fe% After Leaching	Ref.
$Al_2O_3+Fe_2O_3$	HCl, 6.0	60	6	300	125–250	–	12.94	1.33	[29]
Vermiculite	HCl,2.0	80	2	–	500	440	6.26	0.28	[30]
$MnO_2+Fe_2O_3$	HCl 6.36	70	1	–	125	90	0.74	0.07	[31]
WO_3+Fe	HCl 2.0	80	2	900	−200	100	4.40	2.11	[32]
MoO_2+Fe oxide	HCl+HF %5 wt	120	–	1500	–	200	2.93	0.46	[33]
$BaTa_2O_6+Fe$	HCl 12	105	3	300	11.84	40	10.36	2.50	This work

and Ta_2O_5 content of the powder were near to the theoretical values (25 wt% BaO, 75 wt% Ta_2O_5). However, the milled powder also contained a high amount of iron oxide which was around 11%. In addition to iron, the powder also contained ~1.6% Cr and ~0.8% Ni which was due to stainless steel milling vial and balls. EDS analysis of this powder confirmed the XRF results giving ~25 wt% BaO, ~75 wt% Ta_2O_5 which were found by recalculation of original values and 10.36% iron oxide. In order to remove the iron from $BaTa_2O_6$ powder, the milled powder was leached using 6 and 12 M hydrochloric acid at 95 °C and 105 °C for various time periods between 1 and 15 h. EDS analysis of the leached samples indicated that most of the iron was removed just after 1 h of leaching but then the removal of iron did not change considerably even after 15 h of leaching (Fig. 1).

The iron content of 10.36% before leaching decreased sharply to 2.99–4.48% after 1 h indicating that between 56% and 73% of iron was removed depending on leaching conditions. Increasing the leaching time to 15 h led to an iron removal of 70–82% with an iron content of 1.97–3.16%. These results indicated that the maximum iron content that can be removed from $BaTa_2O_6$ was 81% even after 15 h at 105 °C using 12 M HCl. The effect of temperature on iron removal was more significant than acid concentration. Although 6 and 12 M HCl had identical effects on iron removal, temperature (95 and 105 °C) had a more pronounced effect. In addition, approximately 50 wt% of Cr and nearly all of the Ni were dissolved after leaching. EDS results specified that the optimum leaching conditions for iron removal were determined as leaching time of 3 h, HCl molarity of 12 M and temperature of 105 °C. At these optimum conditions, the iron content of $BaTa_2O_6$ decreased to 2.5% indicating a 76% reduction.

The morphology of the leached powders was examined by SEM to reveal how the powders were affected by the acid leaching (Fig. 2). It was believed that micropores were formed before the formation of mesopores during leaching. It was reported in the literature that at the initial

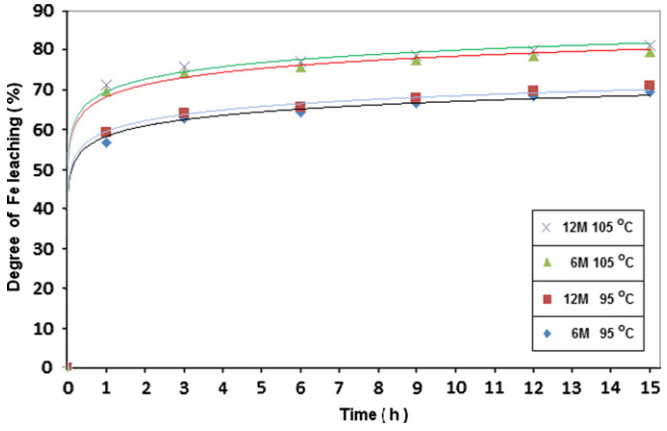

Fig. 1. Dissolution of iron from barium tantalate powder depending on leaching time.

stages of the leaching process, micropores with a diameter less than 2 nm start to form on the surfaces [36] and they grow in size below 50 nm in diameter converting to mesopores and eventually form macropores with a diameter larger than 50 nm. In addition, the diameter of micropores decreased going from the surface down to deeper regions depending on the leaching time [36]. The high removal rate of iron at the beginning of the leaching

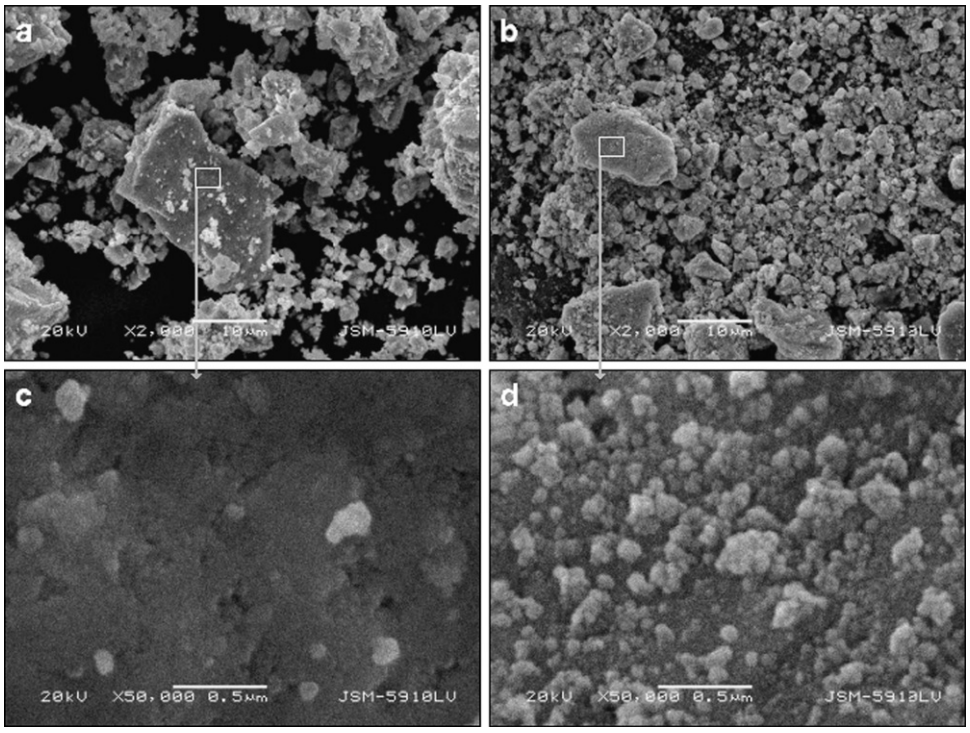

Fig. 2. SEM micrographs of powders before (a and c) and after (b and d) leaching at low and high magnifications.

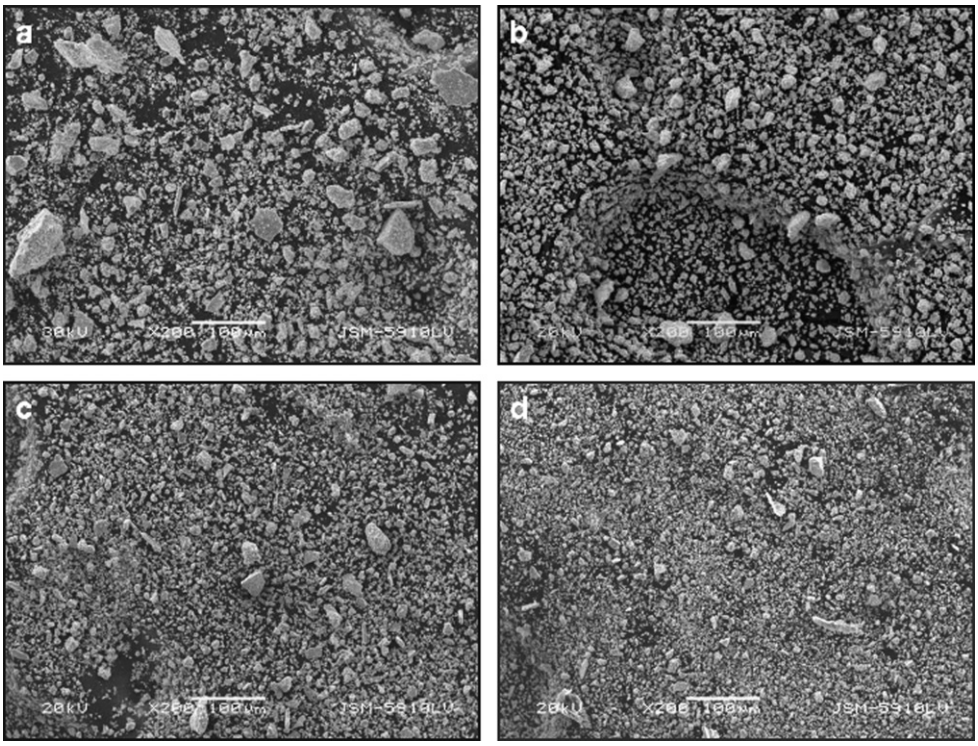

Fig. 3. Effect of leaching time on the agglomeration and morphology of particles: (a) milled powder without leaching, (b) 1 h leaching, (c) 3 h leaching and (d) 15 h leaching at 12 M, 105 °C.

process was possibly due to micropores formed on the surface and also due to low activation energy for dissolution. However, the deceleration of micropore formation and the increase in activation energy in the deeper regions could depress the dissolution of iron from $BaTa_2O_6$.

As the leaching time increased the agglomerates in the powder were dispersed due to leaching effect which led to the formation of finer particles (Fig. 3). During high energy milling, long milling times resulted in the formation of new surfaces and this caused unification of particles and eventually growth of the particle size [14]. The iron contamination which increased with milling time was higher especially along these new surfaces (Fig. 4). During leaching process, HCl possibly penetrates into these new surfaces and decreases the iron impurities by dissolving them and also reduces the particle size by disintegrating the particles.

Although significant amount of iron has been removed by acid leaching, a certain amount of iron remained in the powder. EDS results disclosed that the remnant Fe content was between 1.97% and 3.16% after 15 h of leaching. Increasing the leaching time did not cause a significant decrease in Fe content showing that the iron removal did not increase considerably by leaching time even at longer durations. The fractures and macropores formed on the surfaces were the possible reason for the high remnant iron content. SEM micrographs of leached powder indicated fractures and macropores with diameters larger than 50 nm (Fig. 5). EDS analysis taken from the fracture and

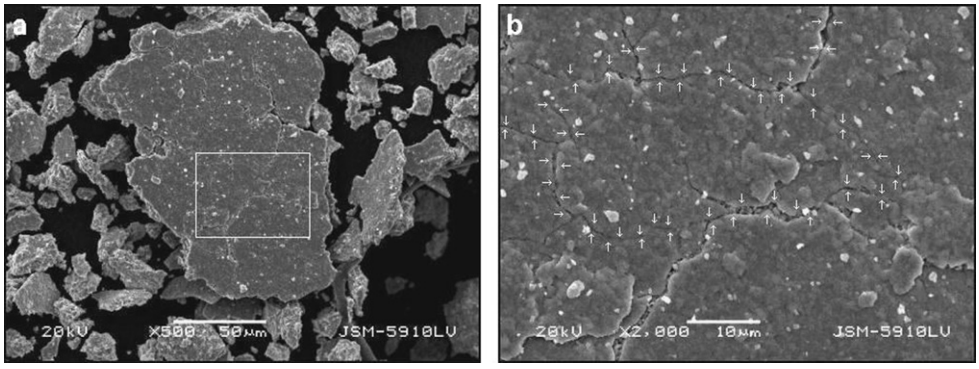

Fig. 4. SEM micrographs of milled powders indicating the boundaries where acid penetrated into and disintegrated the clusters: (a) × 500 and (b) × 2000.

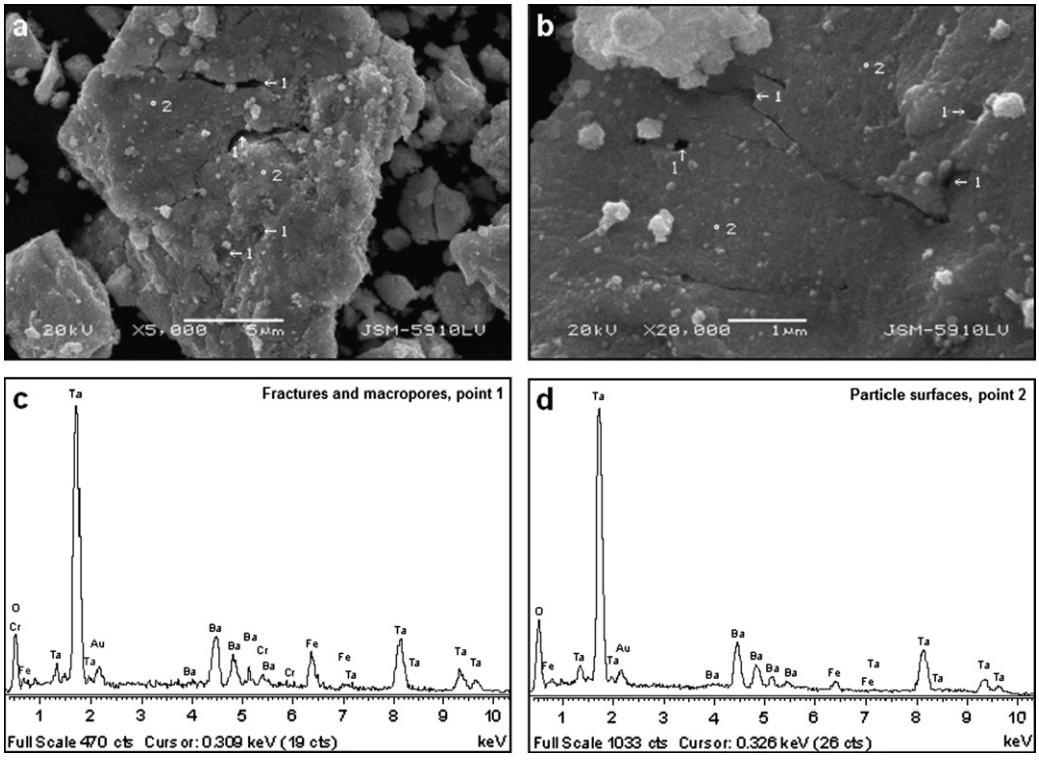

Fig. 5. SEM micrographs of the powders leached for 3 h at 105 °C at 12 M with EDS analysis taken from fractures and micropores (point 1) and from the surfaces (point 2).

macropores (point 1) indicated higher Fe content than the surface of the particles (point 2). The high iron content along the fractures and porosities revealed that the iron impurity remained within these fractures and porosities and cannot be removed by acid leaching possibly due to the mechanochemical oxidation of Fe to Fe_2O_3 during the milling procedure in air, followed most probably with further mechanochemical reactions between Fe_2O_3 and $BaCO_3$–Ta_2O_5 mixture [37–39].

XRD analysis of mechanochemically synthesized powder showed only single phase $BaTa_2O_6$ having tetragonal tungsten bronze (TTB) structure [2,12], (Fig. 6). Leaching of $BaTa_2O_6$ did not cause any change on the XRD peaks revealing no structural change occured during leaching. However, the background of the XRD pattern became smoother after 1 h of leaching revealing that the

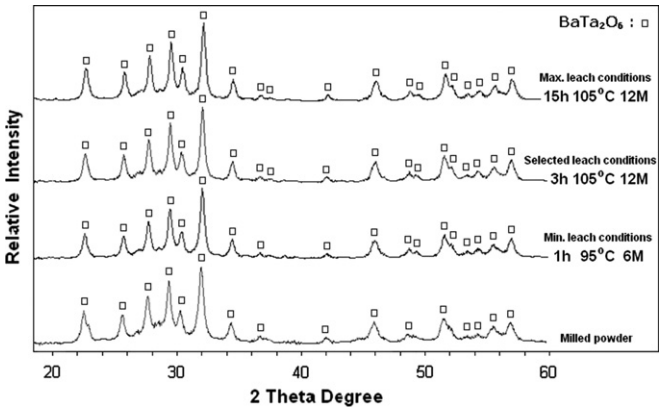

Fig. 6. XRD pattern of milled powder before and after HCl leaching.

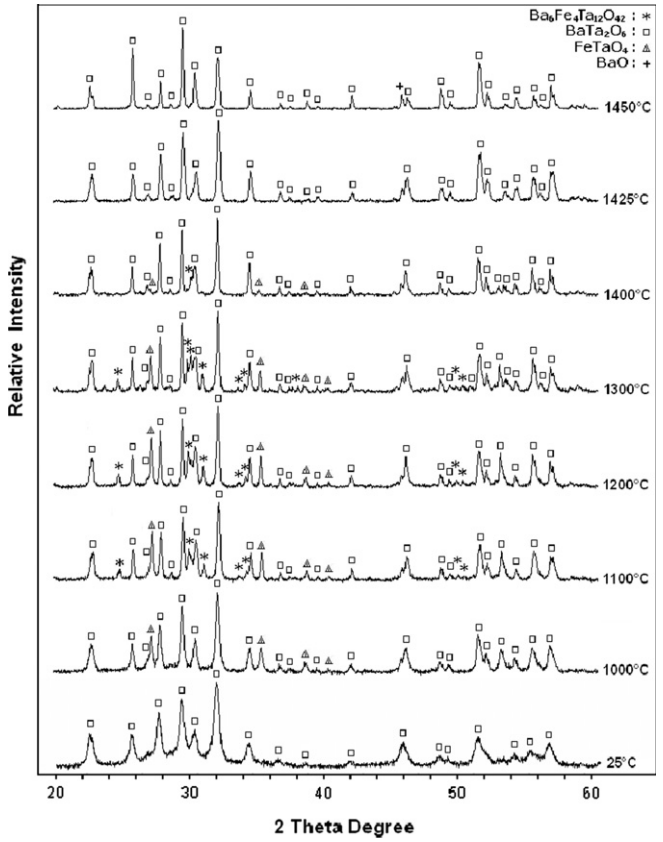

Fig. 7. XRD pattern of milled and leached powder sintered at various temperatures for 5 h.

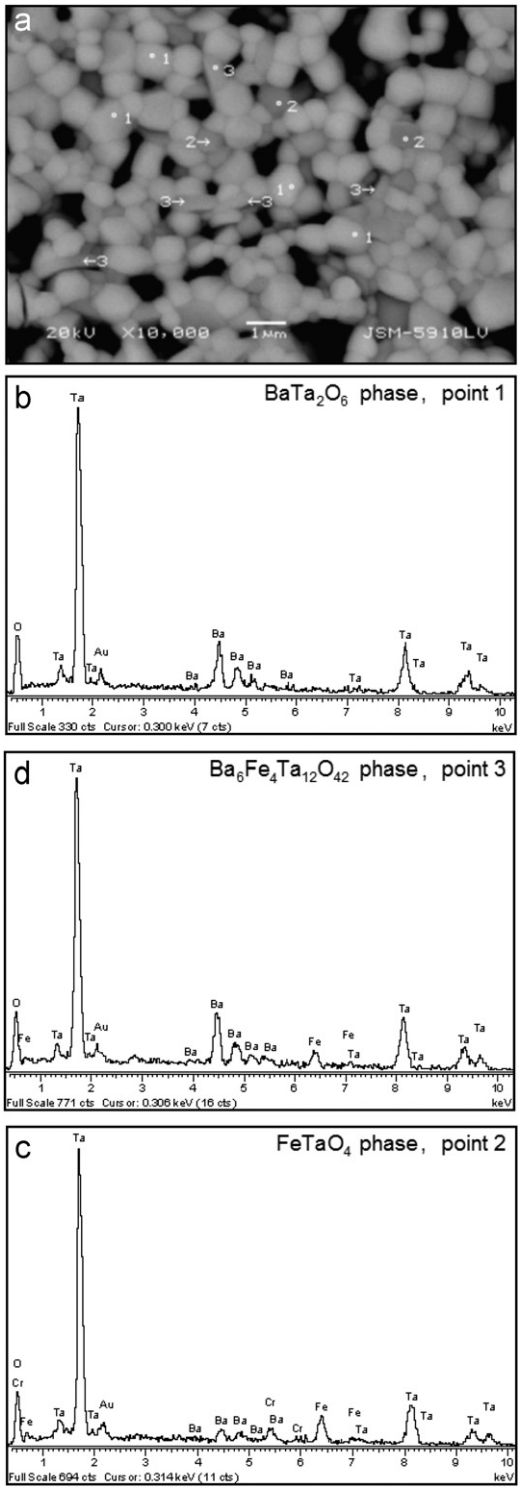

Fig. 8. (a) SEM micrograph of $BaTa_2O_6$ sample sintered at 1300 °C for 5 h after milling and leaching with EDS analysis from (b) $BaTa_2O_6$ grains (point 1), (c) $FeTaO_4$ phase (point 2) and (d) $Ba_6Fe_4Ta_{12}O_{42}$ phase (point 3).

amorphous part of the powder has been removed by acid leaching. But longer leaching times did not cause any further changes on the background probably due to removal of most of the amorphous part at the beginning of the leaching.

3.2. Sintering of leached $BaTa_2O_6$ powder

$BaTa_2O_6$ pellets made from leached powder were sintered between 1000 °C and 1450 °C for 5 h to observe the crystallization, phase development and density behavior.

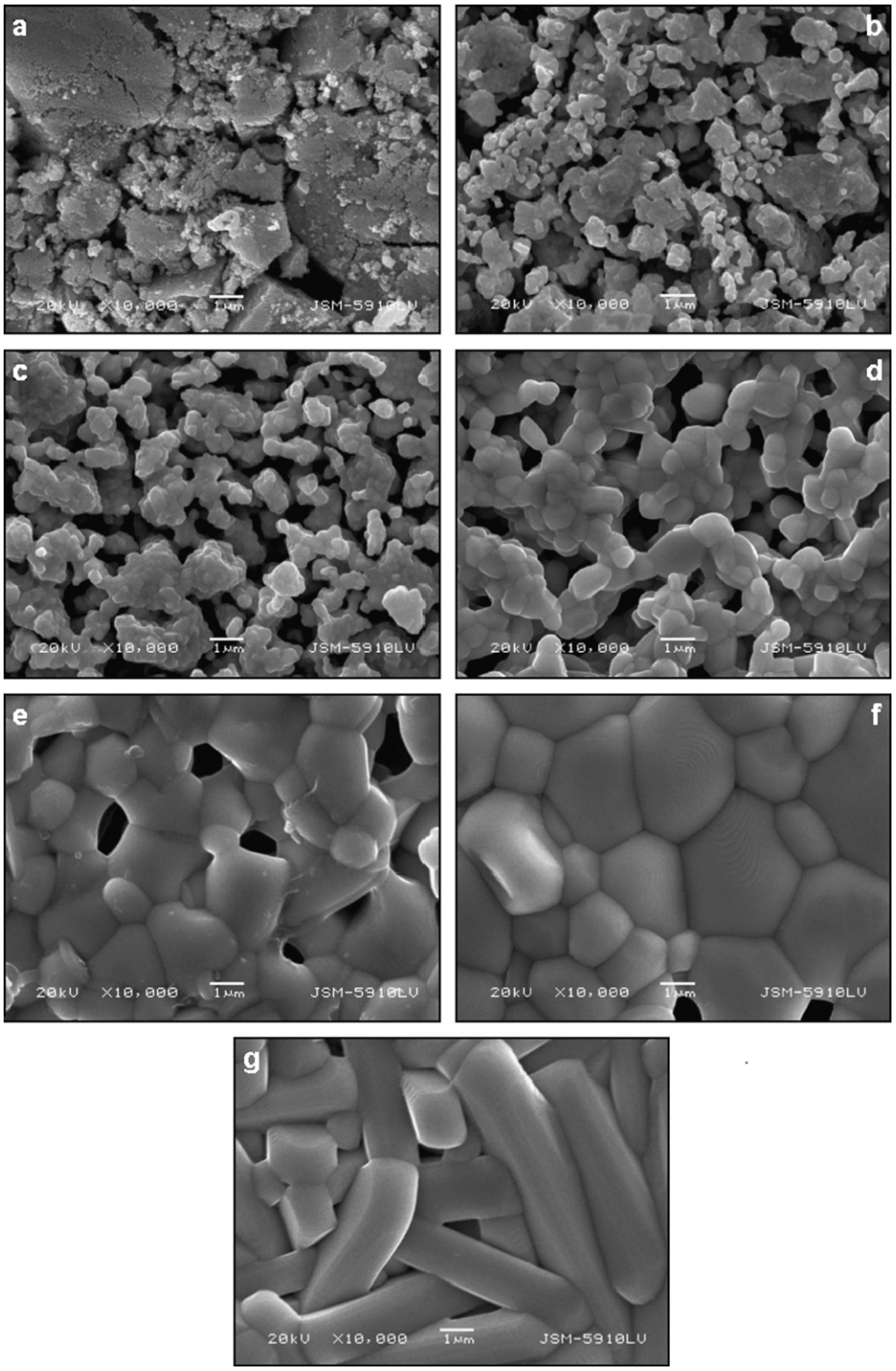

Fig. 9. SEM micrographs of $BaTa_2O_6$ ceramics sintered at various temperatures: (a) 1000 °C, (b) 1100 °C, (c) 1200 °C, (d) 1300 °C, (e) 1400 °C, (f) 1425 °C and (g) 1450 °C, after acid leaching.

Although XRD analysis showed that it contained mainly $BaTa_2O_6$ at 1000 °C, minor amount of $FeTaO_4$ (JCPDS Card no. 43-798) was also observed at this temperature (Fig. 7). However, when the temperature increased to 1100 °C another iron related phase, $Ba_6Fe_4Ta_{12}O_{42}$ (JCPDS Card no. 51-1871), was also detected. These phases were also detected in the SEM (Fig. 8). EDS analysis of these phases were identical with theoretical compositions. As the sintering temperature increased, the peak intensities of these iron related phases decreased and they finally disappeared at 1425 °C. However, these iron related phases were even detected at 1400 °C in minor quantities. XRD pattern of $BaTa_2O_6$ sample sintered at 1425 °C for 5 h included only single phase with tetragonal tungsten bronze (TTB) structure. In addition, BaO second phase (JCPDS Card No. 22-1056) also formed at 1450 °C.

Effect of heat treatment temperature on the grain growth and phase development was investigated by SEM (Fig. 9). The grain sizes and grain shapes at various temperatures are given in Table 3. While the average grain size was at nanometer scale until 1300 °C, it was sharply increased to micron scale levels above 1300 °C. This sharp increase in grain size could be due to the formation of liquid phases. Phase diagrams between barium oxide and iron oxide indicate that liquid phases could occur at low temperatures [40]. XRD indicated that the content of Fe-related phases was high at 1300 °C but they were nearly disappeared at 1400 °C converting mostly to TTB $BaTa_2O_6$ phase and possibly, partly, to a liquid phase. In addition, although the porosity content was high even at 1300 °C, relatively very dense structure was formed at 1425 °C. These results show that probably a liquid phase was formed above 1300 °C

Table 3
Size and shape of $BaTa_2O_6$ grains at various sintering temperatures.

Heat treatment temperature (°C)	Grain shape	Grain size(nm)
1000	Rounded	60–160 nm
1100	Rounded	150–350 nm
1200	Rounded	250–620 nm
1300	Rounded	0.45–1.60 μm
1400	Rounded	0.80–5.00 μm
1425	Rounded	0.90–8.50 μm
1450	Elongated	thickness: 1.10–7.50 μm length: 2.30–76.30 μm

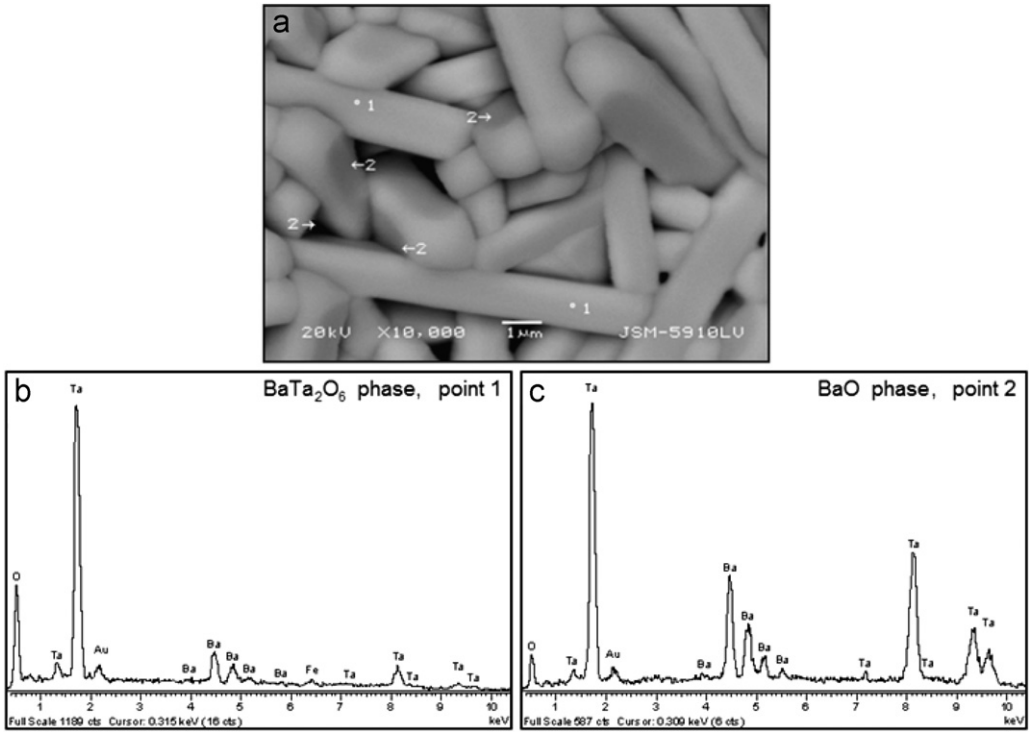

Fig. 10. SEM micrograph and EDS analysis of $BaTa_2O_6$ ceramics sintered at 1450 °C for 5 h after leaching with HCl: (a) SEM at × 10.000, (b) EDS from $BaTa_2O_6$ grains (point 1) and (c) EDS from BaO phase (point 2).

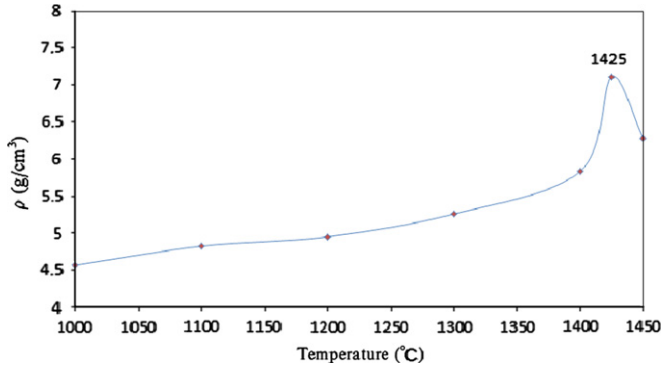

Fig. 11. Variation of density of $BaTa_2O_6$ ceramic produced from leached powder with sintering temperature.

which may increase the grain size and density. The grain morphology was also influenced by the heat treatment temperature in that it was rounded up to 1425 °C but converted to elongated form at 1450 °C. The elongated grains at 1450 °C could be due to a liquid phase and decrease in the BaO content (Fig. 9g).

EDS analysis indicated that Ba:Ta ratio on the $BaTa_2O_6$ grain surfaces was lower than stoichiometric values (point 2 in Fig. 10). This could be due to evaporation of BaO from grains and possibly reprecipitation on the surfaces. The phase diagrams between barium oxide and iron and chromium oxide indicate that liquid phases may form at low temperatures that may accelerate the evaporation of BaO [40].

The variation of density with sintering temperature indicated that the density increased gradually until 1300 °C but then a sharp increase was observed above 1300 °C (Fig. 11). This result reveals a liquid phase formation above 1300 °C. The density reached a maximum at 1425 °C but then decreased with the sintering temperature possibly due to evaporation of liquid. SEM results also showed a dense microstructure at 1425 °C but higher amount of porosity at 1450 °C.

4. Conclusions

Fe contamination due to the milling environment of mechanochemically synthesized $BaTa_2O_6$ ceramic powder showed 81% decrease after leaching by HCl. The iron content decreased from 10.36 wt% to 1.97 wt% for powder leached for 15 h using 12 M HCl at 105 °C. The iron removal indicated a sharp decrease after 1 h of leaching possibly due to low activation energy for dissolution and micropores formed on the surface but then it slowed down with time. The agglomerates in the powder were dispersed due to the leaching effect. Increasing the leaching time did not cause a significant decrease in Fe content probably due to the formation of fractures and macropores on the surfaces. Leaching of barium tantalate removed the amorphous part in the powder without changing the crystal structure. Although iron related second phases were detected in the XRD and SEM at lower temperatures, they disappeared at 1425 °C. $BaTa_2O_6$ grain size was at nanometer scale until 1300°C but it increased to micron scale levels above 1300 °C possibly due to the formation of a liquid phase. Density results also confirmed the liquid phase formation above 1300 °C.

Acknowledgment

We would like to give our great thanks to Marmara University Research Fund (Project nos. FEN-B-110411-0102 and FEN-C-DRP-031210-0296) and Yıldız Technical University Research Fund (Project no. 2011-07-02-DOP-03) for financial support of this investigation.

References

[1] G.K. Layden, Polymorphism of $BaTa_2O_6$, Material Research Bulletin 2 (1967) 533–539.
[2] T.A. Vanderah, R.S. Roth, T. Siegrist, W. Febo, J.M. Loezos, W. Wong-Ng, Subsolidus phase equilibria and crystal chemistry in the system BaO–TiO_2–Ta_2O_5, Solid State Sciences 5 (2003) 149–164.
[3] H. Kato, A. Kudo, New tantalate photocatalysts for water decomposition into H_2 and O_2, Chemical Physics Letter 295 (1998) 487–492.
[4] G.K. Layden, Dielectric and structure studies of hexagonal $BaTa_2O_6$, Material Research Bulletin 3 (1968) 349.
[5] M.R. Hoffmann, S.T. Martin, W. Choi, D.W. Bahnemann, Environmental applications of semiconductor photocatalysis, Chemical Reviews 95 (1995) 69–96.
[6] C. Zhang, Y. Zhu, Synthesis of square Bi_2WO_6 nanoplates as high-activity visible-light-driven photocatalysts, Chemistry of Materials 17 (2005) 3537–3545.
[7] G. Zhang, W. Jiang, S. Yu, Preparation, characterization and photocatalytic property of nanosized K–Ta mixed oxides via a sol–gel method, Materials Research Bulletin 45 (2010) 1741–1747.
[8] E. Bae, W. Choi, Highly enhanced photoreductive degradation of perchlorinated compounds on dye-sensitized metal/TiO_2 under visible light, Environmental Science and Technology 37 (2003) 147–152.
[9] Y.M. Xu, C.H. Langfor, UV- or visible-light-induced degradation of X3B on TiO_2 nanoparticles: the influence of adsorption, Langmuir 17 (2001) 897–902.
[10] K.V. Smith, Alternative dielectrics for GaN HEMTs, Raytheon Technology Today 4 (2007) 8.
[11] N. Shepherd, D.C. Morton, E.W. Forsythe, D. Chiu, The influence of insulator properties on the electro-optical performance flexible ZnS:ErF_3 alternating current thin film electroluminescent devices, Thin Solid Films 515 (2006) 2342–2346.
[12] M. İlhan, A. Mergen, C. Yaman, Mechanochemical synthesis and characterisation of $BaTa_2O_6$ ceramic powders, Ceramics International 37 (2011) 1507–1514.
[13] M. Sherif El-Eskandarany, in: Mechanical Alloying for Fabrication of Advanced Engineering Materials, first edition, Noyes Publications, USA, 2001.
[14] C. Suryanarayana, Mechanical alloying and milling, Progress in Materials Science 46 (2001) 1–184.
[15] G.M. Wang, S.J. Campbell, A. Calka, W.A. Kaczmarek, Synthesis and structural evolution of tungsten carbide prepared by ball milling, Journal of Materials Science 32 (1997) 1461–1467.
[16] E. Yang, C.N.J. Wagner, M.S. Boldrick, The structure of nanocrystalline and amorphous Fe–W, Fe–Mo, and Mn–W alloys prepared by high-energy ball milling, Key Engineering Materials 81–83 (1993) 663–668.
[17] P. Billik, G. Plesch, Mechanochemical synthesis of anatase and rutil nanopowders from $TiOSO_4$, Materials Letters 61 (2007) 1183–1186.

[18] I. Veljković, D. Poleti, M. Zdujić, L. Karanović, Č. Jovalekić, Mechanochemical synthesis of nanocrystalline titanium monoxide, Materials Letters 62 (2008) 2769–2771.
[19] M.A. Roldan, V. López-Flores, M.D. Alcala, A. Ortega, C. Real, Mechanochemical synthesis of vanadium nitride, Journal of the European Ceramic Society 30 (2010) 2099–2107.
[20] Y. Shi, J. Ding, H. Yin, $CoFe_2O_4$ nanoparticles prepared by the mechanochemical method, Journal of Alloys and Compounds 308 (2000) 290–295.
[21] C.B. Reid, J.S. Forrester, H.J. Goodshawb, E.H. Kisi, G.J. Suaning, A study in the mechanical milling of alumina powder, Ceramics International 34 (2008) 1551–1556.
[22] P.P. Chattopadhyay, S.K. Pabi, I. Mana, A metastable allotropic transformation in Nb induced by planetary ball milling, Materials Science and Engineering A304–306 (2001) 424–428.
[23] L.M. Di, H. Bakker, Mechanically induced phase transformation in the Nb_3Au intermetallic compound, Journal of Physics: Condensed Matter 3 (1991) 9319–9326.
[24] M.C. Campbell, G.M. Ritcey, Application of chloride metallurgy to base-metal sulphide and uranium ores at CANMET, Proceedings of Extraction Metallurgy 81 (1981) 76–90.
[25] R. Winand, Chloride-hydrometallurgy, Hydrometallurgy 27 (1991) 285–316.
[26] K.H. Park, D. Mohapatra, B.R. Reddy, A study on the acidified ferric chloride leaching of a complex (Cu–Ni–Co–Fe) matte, Separation and Purification Technology 51 (2006) 332–337.
[27] A.K. De, S.M. Khopkar, R.A. Chalmers, in: Solvent Extraction of Metals, first ed., Van Nostrand-Reinhold, London, 1970.
[28] M. Tanaka, Chemistry of Solvent Extraction, Kyoritsu, Tokyo, 1977.
[29] A. Mergen, Pruduction of sintered high alumina refractories from Turkish bauxite ore, British Ceramic Transactions 103 (2004) 42–46.
[30] J. Temuujin, K. Okada, J.D. MacKenzie, Preparation of porous silica from vermiculite by selective leaching, Applied Clay Science 22 (2003) 187–195.
[31] Y. Darmane, M. Cherkaoui, S. Kitane, A. Alaoui, A. Sebban, M. Ebn Touhami, Preparation of chemical manganese dioxide from Moroccan pyrolusite mine waste, Hydrometallurgy 92 (2008) 73–78.
[32] S. Gürmen, S. Timur, C. Arslan, I. Duman, Acidic leaching of scheelite concentrate and production of hetero-poly-tungstate salt, Hydrometallurgy 51 (1999) 227–238.
[33] M. Kumar, M.N. Babu, T.R. Mankhand, B.D. Pandey, Precipitation of sodium silicofluoride (Na_2SiF_6) and cryolite (Na_3AlF_6) from HF/HCl leach liquors of alumino-silicates, Hydrometallurgy 104 (2010) 304–307.
[34] F.X. Le Bourdonnec, G. Poupeau, C. Lugliè, SEM–EDS analysis of western Mediterranean obsidians: a new tool for Neolithic provenance studies, Computes Rendus Geoscience 338 (2006) 1150–1157.
[35] G. Poupeau, F.X. Le Bourdonnec, T. Carter, S. Delerue, M.S. Shackley, J.A. Barrat, S. Dubernet, P. Moretto, T. Calligaro, M. Milic, K. Kobayashi, The use of SEM–EDS, PIXE and EDXRF for obsidian provenance studies in the Near East: a case study from Neolithic Çatalhöyük (central Anatolia), Journal of Archaeological Science 37 (2010) 2705–2720.
[36] H. Yang, C. Du, Y. Hu, S. Jin, W. Yang, A. Tang, E.G. Avvakumov, Preparation of porous material from talc by mechanochemical treatment and subsequent leaching, Applied Clay Science 31 (2006) 290–297.
[37] G.R. Karagedov, N.Z. Lyakhov, Preparation and sintering of nanosized alpha-Al_2O_3 powder, Nanostructured Materials 11 (1999) 559–572.
[38] G.R. Karagedov, E.A. Ryzhikov, S.S. Shatskaya, Peculiarities of α-Al_2O_3 and ZrO_2 nano-comminuting, Chemistry for Sustainable Development 10 (2002) 47–56.
[39] G.R. Karagedov, N.Z. Lyakhov, Mechanochemical grinding of inorganic oxides, KONA Powder Particle Journal 21 (2003) 76–87.
[40] TDnucl–Thermodata Nuclear Phase Diagrams.